J Eng Math (2007) 57:181–198
DOI 10.1007/s10665-006-9073-y

ORIGINAL PAPER

Regularization of inverse heat conduction by combination of rate sensor analysis and analytic continuation

Jay I. Frankel

Received: 8 February 2006 / Accepted: 3 July 2006 / Published online: 24 November 2006
© Springer Science+Business Media B.V. 2006

Abstract This paper describes some recent observations associated with (1) clarifying and expanding upon the integral relationship between temperature and heat flux in a half-space; (2) offering an analytic-continuation approach for estimating the surface temperature and heat flux in a one-dimensional geometry based on embedded measurements; and, (3) offering a novel digital filter that supports the use of analytic continuation based on a minimal number of embedded sensors. Key to future inverse analysis must be the proper understanding and generation of rate data associated with both the temperature and heat flux at the embedded location. For this paper, some results are presented that are theoretrically motivated but presently adapted to implement digital filtering. A pulsed surface heat flux is reconstructed by way of a single thermocouple sensor located at a well-defined embedded location in a half space. The proposed low-pass, Gaussian digital filter requires the specification of a cut-off frequency that is obtained by viewing the power spectra of the temperature signal as generated by the Discrete Fourier Transform (DFT). With this in hand, and through the use of an integral relationship between the local temperature and heat flux at the embedded location, the embedded heat flux can be accurately estimated. The time derivatives of the filtered temperature and heat flux are approximated by a simple finite-difference method to provide a sufficient number of terms required by the Taylor series for estimating (i.e., the projection) the surface temperature and heat flux. A numerical example demonstrates the accuracy of the proposed scheme. A series of appendices are offered that describe the mathematical details omitted in the body for ease of reading. These appendices contain important and subtle details germane to future studies.

Keywords Digital filtering · Inverse problems · Parabolic equations

1 Introduction

The precise measurement of temperature and heat flux [1, pp. 502–577], [2,3], [4, pp. 285–354] are basic quantities of interest in heat transfer. These quantities have been traditionally sought and numerous sensors have been developed capable of producing accurate results over various conditions, applications and

J. I. Frankel (✉)
Mechanical, Aerospace and Biomedical Engineering Department, University of Tennessee,
414 Dougherty Engineering Bldg, Knoxville, TN 37996-2210, USA
e-mail: vfrankel@earthlink.net

thermal ranges. High temperature, heat fluxes and heating/cooling rates are of practical concern, owing to their appearance in aerospace, defense and nuclear applications. Reentry involving minutes of exposure and direct-energy impingement involving seconds of exposure are high-temperature and heat-flux applications. Many applications preclude the use of surface-mounted sensors. Often complex mathematical devices are required to project data from an embedded location to obtain stable surface information. This process is often mathematically ill-posed, that is, small errors in data at the measurement site magnify (unstable) in the projection to the desired surface site [5, pp. 221–242], [6, pp. 7–22], [7, pp. 51–101], [8, pp. 27–65], [9, pp. 67–76], [10, pp. 963–979]. The inverse heat-conduction problem has been considered by many researchers. However, to date, regularization methods have relied on mathematical devices that require the specification of a "regularization-type" parameter. The optimal value of this parameter is often difficult to acquire and affects the quality of the prediction. Frankel and colleagues [11–17] have taken a different point of view. Through analysis, they have identified the culprits in the projection process. With this information, it is now important to move away from the concept of measurements solely based on temperature and heat flux. Rate information, involving the time derivative, have been shown a key element for the accurate projection. Either one should develop rate-based sensors or develop digital filters that assure the proper smoothness in the time derivative in both temperature and heat flux. This paper describes a filtering process used in conjunction with analytic continuation (i.e., Taylor series [16]) that can reconstruct surface heat fluxes with remarkable accuracy using trivial numerical methods.

2 Mathematical formulations

In this section, various heat-conduction relationships are developed in the context of half-space heat conduction. This geometry should not be viewed as academic, since in many short-time situations the back surface remains at the initial condition. The conventional (infinite speed of thermal propagation), linear heat equation [18, Chapter 1] in temperature for the half-space is

$$\rho C \frac{\partial T}{\partial t}(x,t) = k \frac{\partial^2 T}{\partial x^2}(x,t), \quad (x,t) \geq 0, \tag{1a}$$

where the penetrating surface heat flux $q''(0,t)$, which is often the most desirable quantity of interest, is expressible in terms of surface temperature through Fourier's law as

$$q''(0,t) = -k \frac{\partial T}{\partial x}(0,t), \tag{1b}$$

at $x = 0$ where k is the thermal conductivity, C is the heat capacity, and ρ is the density. Equation 1a is subject to the initial condition

$$T(x,0) = 0 \quad x \geq 0. \tag{1c}$$

The initial condition is specified as 0, since one could readily use the linear transformation $\theta(x,t) - T_o = T(x,t)$ to impose the trivial initial condition in the modified variable (also $\partial\theta/\partial t = \partial T/\partial t$).

As an important aside, expressing the heat equation shown in Eq. 1a as two first-order equations based on the first law of thermodynamics (general law) and Fourier's law (particular law)

$$\rho C \frac{\partial T}{\partial t}(x,t) = -\frac{\partial q''}{\partial x}(x,t), \tag{1d}$$

$$q''(x,t) = -k \frac{\partial T}{\partial x}(x,t), \tag{1e}$$

respectively, is highly useful and revealing in many applications [19]. It is possible to express the heat equation in heat flux, $q''(x,t)$ as

$$\frac{1}{\alpha} \frac{\partial q''}{\partial t}(x,t) = \frac{\partial^2 q''}{\partial x^2}(x,t), \quad (x,t) \geq 0, \tag{1f}$$

by merely eliminating, under appropriate mathematical assumptions, the temperature between the two first-order equations. Here, α is the thermal diffusivity given as $\alpha = k/(\rho C)$.

The simplest approach to implement in order to arrive at the first preliminary analytic result, i.e., the solution, involves the Fourier-cosine Transform. Let the transform pair [20] be defined as

Transform:

$$\bar{T}_\lambda(t) = \sqrt{\frac{2}{\pi}} \int_{x=0}^{\infty} T(x,t)\cos(\lambda x)\mathrm{d}x, \quad (\lambda, t) \geq 0, \tag{2a}$$

Inversion:

$$T(x,t) = \sqrt{\frac{2}{\pi}} \int_{\lambda=0}^{\infty} \bar{T}_\lambda(t)\cos(\lambda x)\mathrm{d}\lambda, \quad (x,t) \geq 0. \tag{2b}$$

Implementing this approach [20] is conventional and leads to the classical integral solution

$$T(x,t) = \sqrt{\frac{1}{\rho C k \pi}} \int_{u=0}^{t} q''(0,u) \frac{\mathrm{e}^{-\frac{x^2}{4\alpha(t-u)}}}{\sqrt{t-u}}\mathrm{d}u, \quad (x,t) \geq 0. \tag{3a}$$

Equation 3a displays the relationship between the surface heat flux ($x = 0$) and the temperature anywhere within the half space ($x \geq 0$). That is, the solution to the heat equation, when provided the boundary heat flux, is known from (3a). Operating on (3a) with $-k\frac{\partial}{\partial x}$ and making use of the definition of Fourier's heat flux shown in (1e) produces

$$q''(x,t) = \sqrt{\frac{x^2}{4\alpha\pi}} \int_{u=0}^{t} q''(0,u) \frac{\mathrm{e}^{-\frac{x^2}{4\alpha(t-u)}}}{(t-u)^{\frac{3}{2}}}\mathrm{d}u, \quad x > 0, \ \ t \geq 0, \tag{3b}$$

where $\alpha = k/(\rho C)$. Equation 3a relates the heat flux, $q''(x,t)$, at any arbitrary x to the surface heat flux, $q''(0,t)$. Given the surface heat flux, $q''(0,t)$, a mere numerical integration is required to obtain the heat flux at any position in the half space. The kernel in (3b) is non-singular for $x > 0$ at $u = t$ from L'Hôpital's rule [21, p. 604]. A potential inverse statement would be to determine the surface heat flux, $q''(0,t)$, when provided the heat flux at arbitrary x, namely, $q''(x,t)$. Thus, Eq. 3b is a first-kind integral equation for the surface heat flux and is known to be highly ill-posed.

2.1 Surface measurement inverse problem-review

Next, we evaluate (3a) at $x = 0$ to obtain

$$T(0,t) = \sqrt{\frac{1}{\rho C k \pi}} \int_{u=0}^{t} \frac{q''(0,u)}{\sqrt{t-u}}\mathrm{d}u, \quad t \geq 0. \tag{4}$$

Equation 4 can be interpreted as (i) an integral for obtaining the surface temperature when provided the surface heat flux or (ii) an Abel integral equation for the surface heat flux when provided the surface temperature. The latter computation is unstable to discrete noisy surface-temperature data, while the former is numerically stable. Abel's equation permits analytic inversion by classical regularization as associated with singular integral equations [14]. Inversion leads to

$$q''(0,t) = \sqrt{\frac{\rho C k}{\pi}} \int_{u=0}^{t} \frac{\partial T}{\partial u}(0,u) \frac{\mathrm{d}u}{\sqrt{t-u}}, \quad t \geq 0. \tag{5}$$

This formulation indicates the ill-posedness of the process based on discrete, noisy temperature measurements, since it involves numerical differentiation of data which is known to be ill-posed [17,22,23].

Frankel and Arimilli [24] showed that the root-mean-square (RMS) surface heat-flux error grows as $\sqrt{N}$ (for large N) if the simulated data are based on white noise as expressed through

$$T_i = T(0,t_i) + \gamma \| T(0,t) \|_\infty u_i, \quad i = 1,2,\ldots,N, \tag{6}$$

where we impose exactness on the initial condition, namely $T_\mathrm{o} = T(0, t = 0) = 0$. Here, $T(0,t_i)$ represents the numerically "exact" solution at time, t_i, γ is the noise factor, u_i is the ith random number drawn as generated from a uniform probability-density function in the interval $[-1,1]$, and $\|g(t)\|_\infty = \max_{t\in[0,t_\mathrm{max}]} |g(t)|$ for the real function $g(t)$.

The required integral relationship between the surface temperature and heat flux can be derived by numerous methods including: (a) Fourier-cosine Transforms [20], (b) Green's Functions [25, pp. 42–86], (c) Method of Kulish [26,27] and (d) Taylor Series [24]. Kulish and colleagues [26,27] investigated several transient, linear, half-space heat-transfer problems and developed novel integral relationships between the temperature and heat flux for any location x in the half-space. This local relationship (not solution) is quite useful in the half-space investigations considered by Kulish and his colleagues. Their integral relationship permits two distinct interpretations. The first is direct and stable, while the second is inverse and normally unstable (depending on the data space). The first involves the specification of the local heat flux from which the local temperature is determined. This statement only requires the implementation of integration. The second involves the specification of temperature from which the local heat flux is reconstructed. This situation leads to a Volterra integral equation of the first kind. If discrete, noisy temperature data are specified, this formulation is unstable.

Kulish et al. [26,27] developed the relationship using Laplace transforms. This mathematical procedure is actually somewhat limited. That is, the identical relationship can be obtained directly from (3a) as described in Appendix A. Equation 3a, as developed from a Fourier-cosine transform, is basically equivalent to using a half-space Green's function approach. Appendix B is particularly revealing and general for acquiring both the integral relationship between temperature and heat flux and also reveals the hypersingular nature of the surface problem. The derivation proposed in Appendix B is general and useful to other geometries [28]. Appendix C is offered for introducing the reader to hypersingular integral equations and the resulting kernel that is formed for the surface problem described in Appendix B. In fact, Frankel [28] has demonstrated that the full-space Green's function formulation (i.e., a boundary-element formulation) actually offers additional insight into this integral relationship between heat flux and temperature in one-dimensional problems. The integral relationship between the temperature and heat flux is (for the sake of generality, $T(x,0) = T_\mathrm{o}$, for the moment)

$$T(x,t) = T_\mathrm{o} + \frac{1}{\sqrt{\pi\rho Ck}} \int_{u=0}^{t} q''(x,u) \frac{\mathrm{d}u}{\sqrt{t-u}}, \quad x,t \geq 0. \tag{7a}$$

At the surface ($x = 0$), Eq. 7a reduces to (4). Again, if temperature data are provided at arbitrary position, x, Eq. 7a indicates that an Abel integral equation for the corresponding heat flux results. This again, leads to an ill-posed problem. Analytic inversion, whose details are given in Appendix A via regularization associated with weakly singular integral equations, of Equation 7a leads to

$$q''(x,t) = \sqrt{\frac{\rho Ck}{\pi}} \int_{u=0}^{t} \frac{\partial T}{\partial u}(x,u) \frac{\mathrm{d}u}{\sqrt{t-u}}, \quad x,t \geq 0, \tag{7b}$$

which again indicates the importance of the local heating/cooling rate, $\frac{\partial T}{\partial t}(x,t)$, on stabilizing the heat flux, $q''(x,t)$. In fact, specification of heating/cooling rate data containing white noise leads to a decay in the RMS of the local heat-flux error as the sample density increases (the RMS decays as $\sqrt{\log(N)/N}$ as N grows). This implies a well-posed statement! Equations 7a and 7b have direct application to measurements in constant-property materials (in this case in the half-space geometry). Equation 7b implies that a mere temperature measurement from a single probe can provide the local heat flux if performed carefully to assure the proper heating/cooling rate, $\mathrm{d}T/\mathrm{d}t$!

As an aside, Eq. 7a can quickly become (7b) through the use of the previously noted first-order representation (i.e., Eq. 1d, 1e) of the heat equation. That is, operate on (7a) with $-k\frac{\partial}{\partial x}$. The LHS now becomes $q''(x,t)$ by Fourier's law and the $\frac{\partial q''}{\partial x}$ term in the integral can be viewed as $-\rho C\frac{\partial T}{\partial u}$ and, thus, Eq. 7b is obtained without use of applied mathematics.

2.2 Inverse heat-conduction problem

Given measurements at the embedded location, $x = \eta > 0$ in the half-space, determine the surface temperature, $T(0,t)$, and corresponding conductive heat flux, $q''(0,t)$. This is a highly ill-posed problem if provided embedded temperature, $T(\eta,t)$ and heat flux, $q''(\eta,t)$, data. This is observable from the first-kind integral equations displayed in (3a) and (3b). In the present context, it is our intention to show how to implement digital filtering which has a stabilizing effect when an appropriate cut-off frequency is defined. The physical nature of diffusion theory at the embedded site should naturally damp out high-frequency components. When a measurement contains spurious high-frequency components, these components will play havoc on derivatives and thus can and should be removed using specialized low-pass filters.

3 Data preprocessing: discrete Fourier transforms (DFT) and digital filtering

The major computational issue for many inverse problems lies in either the explicit or implicit need to numerically differentiate noisy discrete data. High-frequency components in this calculation often play havoc on the predictions; and, in many physical problems should not even be present. Data analysis should involve a clear understanding of the signal-to-noise ratio in the frequency domain. Once the signal falls into the noise domain, it is unreasonable to use these high-frequency components for useful reconstruction. Low-pass filtering of data provides a simple and logical manner for reducing the effects of unwanted high-frequency components.

3.1 Background: DFT

The discrete Fourier transform (DFT) [29, pp. 23–33] is used to define a cut-off (or critical) frequency for removing unwarranted high-frequency modes. This is in-line with Weiner filtering concepts [30, pp. 417–423] (see Fig. 1 for a qualitative understanding) and provides general guidance into defining the cut-off frequency.

Frequency content in the signal above the cut-off frequency should be minimized and not propagated into the differentiation. The proposed Gauss low-pass filter utilizes this cut-off frequency, (f_c), and this value is directly incorporated into the mathematical description of the digital filter. The cut-off frequency is approximated by visual inspection of the amplitude (power) spectrum of the signal data. The DFT of the data is defined as

$$\hat{T}(\omega_n) = \sum_{k=0}^{N-1} T(t_k)\mathrm{e}^{\frac{-2\pi ink}{N}}, \quad n = 0,1,\ldots,N-1, \tag{8a}$$

with formal inversion

$$T(t_k) = \frac{1}{N}\sum_{n=0}^{N-1} \hat{T}(\omega_n)\mathrm{e}^{\frac{2\pi ink}{N}}, \quad k = 0,1,\ldots,N-1. \tag{8b}$$

For power-spectrum analysis, we define

$$a_n = \sum_{k=0}^{N-1} T(t_k)\cos\left(\frac{2\pi nk}{N}\right), \quad n = 0,1,\ldots,N-1, \tag{8c}$$

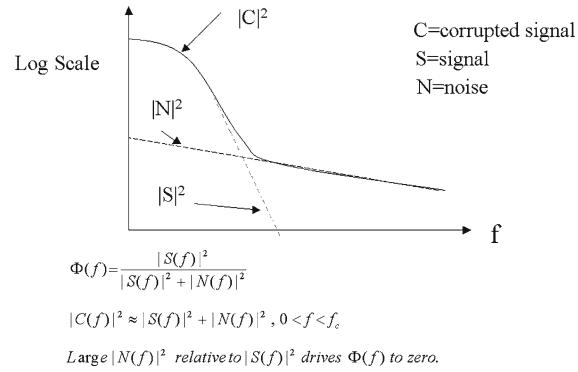

Fig. 1 Signal/noise ratio and the optimal (Weiner) filter, $\Phi(f)$

$$b_n = \sum_{k=0}^{N-1} T(t_k) \sin\left(\frac{2\pi nk}{N}\right), \quad n = 0, 1, \ldots, N-1, \tag{8d}$$

where we define the power density as

$$c_n = \sqrt{a_n^2 + b_n^2}, \tag{8e}$$

or the modified power density as

$$C_n = \frac{2}{N} c_n, \tag{8f}$$

for graphical convenience.

Thus, the power density resulting from the DFT for the data displayed is of considerable importance. An extrapolated straight line, as generated using the flat or large n region, can be developed under appropriate assumptions for estimating the noise. The cut-off point, n_c, is defined as the location of coalescence for the power density and the extrapolated straight lines associated with small and large values of n. This will be graphically clarified in the coming sections. In fact, there is sufficient flexibility in this numerical value for implementation [24]. For conduction applications, this spectrum often decays rapidly (several orders of magnitude) to form a near linear segment. In this linear segment of the spectrum, involving high-frequency components, it is often difficult to discern the difference between the signal and noise, and thus should be eliminated or minimized.

3.2 Background: digital filtering

A Gauss filter function for temperature can be devised using Fourier convolution principles. The advantage of such a filter lies in its behavior in both the time and frequency domains. The Fourier transform of a Gauss function produces another Gauss function (i.e., self-reciprocal). Thus, in both time and frequency, the functions are wiggle-free. This low-pass filter offers good differentiability properties. The finite number of samples in the original data set now becomes continuous and could provide additional flexibility when incorporated into numerical schemes, since one is not restricted to using the exact sample times. As a comparison with the classical low-pass filter [31, p. 79] (constant up to the cut-off frequency and then zero beyond), Fig. 2 presents some qualitative details for choosing the low-pass Gauss filter for the present investigation. Again, the mathematics suggest that we be highly cognizant of the derivative of the temperature data.

As previously suggested, it is desirable to have a filter in the frequency domain that does not contain "wiggles", i.e., sidelobes. For the moment, let the filter in the frequency domain be given as

$$\hat{f}(\omega) = \mathrm{e}^{-(\frac{\omega}{\omega_c})^2}, \tag{9}$$

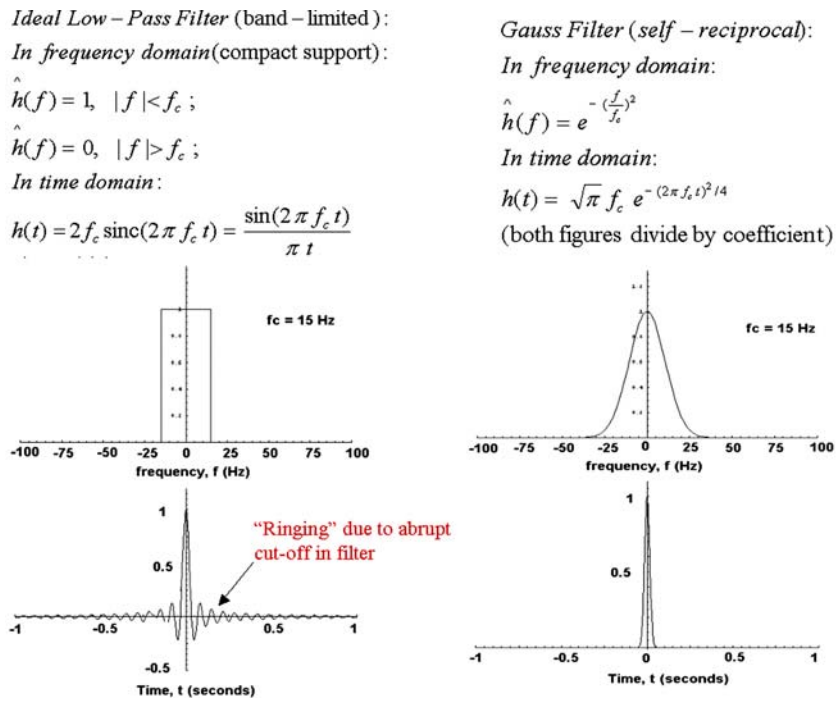

Fig. 2 Comparison between low-pass filter and proposed low-pass Gauss filter in both frequency and time domains

where $\omega = 2\pi f$. In the discrete sense, the angular frequency is $\omega_n = 2\pi n/t_{\max}$. The resulting inverse Fourier transform of (9) is

$$f(t) = \frac{\omega_c}{2\sqrt{\pi}} \mathrm{e}^{-\frac{t^2\omega_c^2}{4}}. \tag{10}$$

From the convolution property of the Fourier transform, we obtain

$$\bar{T}_{\text{filtered}}(t) = \frac{\sum_{n=0}^{N-1} T(t_n) \mathrm{e}^{-\frac{(t-t_n)^2\omega_c^2}{4}}}{\sum_{n=0}^{N-1} \mathrm{e}^{-\frac{(t-t_n)^2\omega_c^2}{4}}}. \tag{11}$$

Letting $t \to t_k$ yields

$$\bar{T}_{\text{filtered}}(t_k) = \frac{\sum_{n=0}^{N-1} T(t_n) \mathrm{e}^{-\frac{(t_k-t_n)^2\omega_c^2}{4}}}{\sum_{n=0}^{N-1} \mathrm{e}^{-\frac{(t_k-t_n)^2\omega_c^2}{4}}}, \quad k = 0, 1, \ldots, N-1. \tag{12}$$

The denominator of (12) is nearly constant with exception to the neighborhood of the endpoints. Often, pre- and post-padding of the data set are used to reduce leakage-type effects that occur near the endpoints. For this study, pre- and post-padding are not performed. Also, with some care Eq. 12 can be transformed into a running filter.

4 Taylor series—analytic continuation

Next, using the concept of Analytic Continuation [14] (i.e., Taylor series), one can expose important sensor contributions for inverse analysis.

4.1 Single thermocouple arrangement

To begin, a half-space region is defined containing the embedded location denoted as $x = \eta$. Consider the Taylor-series expansion of the surface temperature $T(0,t)$ about the embedded point $x = \eta > 0$, namely

$$T(0,t) = T(\eta,t) - \frac{\partial T}{\partial x}(\eta,t)\frac{\eta}{1!} + \frac{\partial^2 T}{\partial x^2}(\eta,t)\frac{\eta^2}{2!} - \frac{\partial^3 T}{\partial x^3}(\eta,t)\frac{\eta^3}{3!} + \frac{\partial^4 T}{\partial x^4}(\eta,t)\frac{\eta^4}{4!} \ldots . \tag{13}$$

Equation 13 can be alternatively expressed in various temporal derivatives of the temperature $T(x,t)$ and heat flux $q''(x,t)$ through the particular law describing Fourier's heat conduction $q'' = -k\frac{\partial T}{\partial x}$ and the first law of thermodynamics given by $\rho C\frac{\partial T}{\partial t} = -\frac{\partial q''}{\partial x}$. That is, one can express (13) as

$$T(0,t) = T(\eta,t) + q''(\eta,t)\frac{\eta}{1!k} + \frac{\partial T}{\partial t}(\eta,t)\frac{\eta^2}{2!\alpha} + \frac{\partial q''}{\partial t}(\eta,t)\frac{\eta^3}{3!\alpha k} + \frac{\partial^2 T}{\partial t^2}(\eta,t)\frac{\eta^4}{4!\alpha^2} + \cdots \tag{14}$$

Equation 14 encourages the measurement of $T(\eta,t), q''(\eta,t)$ and their temporal derivatives. A similar Taylor series can be developed for $q''(0,t)$ based on measured quantities at $x = \eta$. In this case, one obtains

$$q''(0,t) = q''(\eta,t) + \frac{k}{\alpha}\frac{\partial T}{\partial t}(\eta,t)\frac{\eta}{1!} + \frac{1}{\alpha}\frac{\partial q''}{\partial t}(\eta,t)\frac{\eta^2}{2!} + \frac{k}{\alpha^2}\frac{\partial^2 T}{\partial t^2}(\eta,t)\frac{\eta^3}{3!} + \frac{1}{\alpha^2}\frac{\partial^2 q''}{\partial t^2}(\eta,t)\frac{\eta^4}{4!} + \cdots . \tag{15}$$

4.2 Two-thermocouple arrangement

Before proceeding, the use of two sensors lined up along the x-axis appears fruitful under appropriate circumstances. Consider the case where two thermocouples are installed along the isotherms at $x = \eta$ and $x = 2\eta$. This concept involves developing two Taylor-series expansions, the first at $x = 0$ about $x = \eta$; and, the second expansion at $x = 2\eta$ about $x = \eta$. Adding these expansions eliminates various terms. This process is commonly used for generating higher-order finite-difference schemes. Doing so yields

$$T(0,t) = -T(2\eta,t) + 2T(\eta,t) + \frac{1}{\alpha}\frac{\partial T}{\partial t}(\eta,t)\eta^2 + O(\eta^4), \quad t \geq 0. \tag{16a}$$

Equation 14, for a single temperature sensor, can be expressed as

$$T(0,t) = T(\eta,t) + q''(\eta,t)\frac{\eta}{1!k} + \frac{\partial T}{\partial t}(\eta,t)\frac{\eta^2}{2!\alpha} + \frac{\partial q''}{\partial t}(\eta,t)\frac{\eta^3}{3!\alpha k} + O(\eta^4), \quad t \geq 0 \tag{16b}$$

for fixed truncation error. Thus, for an identical truncation error, the two-probe system for estimating the surface temperature only requires knowledge of the two sensor temperatures at $x = \eta, 2\eta$ and the heating/cooling rate at $x = \eta$ and does not require the heat flux nor its rate at either site.

Similarly, the heat flux at $x = 0$ based on the proposed two-probe arrangement can be estimated from

$$q''(0,t) = -q''(2\eta,t) + 2q''(\eta,t) + \frac{1}{\alpha}\frac{\partial q''}{\partial t}(\eta,t)\eta^2 + O(\eta^4), \quad t \geq 0. \tag{17a}$$

Equation 15, for a single temperature sensor, can be expressed as

$$q''(0,t) = q''(\eta,t) + \frac{k}{\alpha}\frac{\partial T}{\partial t}(\eta,t)\frac{\eta}{1!} + \frac{1}{\alpha}\frac{\partial q''}{\partial t}(\eta,t)\frac{\eta^2}{2!} + \frac{k}{\alpha^2}\frac{\partial^2 T}{\partial t^2}(\eta,t)\frac{\eta^3}{3!} + O(\eta^4), \quad t \geq 0. \tag{17b}$$

Observe, for common truncation error, a two-probe sensor does not require the second derivative of the temperature at the probe site.

5 Numerics

It is evident from viewing Eqs. 14 and 15 that the goal for estimating the surface temperature, $T(0,t)$ and heat flux, $q''(0,t)$ involves obtaining the RHS of their respective expansions. This involves rate data for both

temperature and heat flux at the embedded location $x = \eta$. For this study, which is based on only having temperature data at $x = \eta$, we now define the numerical procedure for arriving at surface temperature, $T(0,t)$, and heat flux, $q''(0,t)$. In a nutshell, the process is as follows:

- Obtain noisy, temperature data, $T(\eta,t) = T_i, i = 0,1,\ldots,M$, from embedded site.
- Interrogate power spectrum in order to approximate cut-off frequency, f_c, for Gauss filter.
- Filter noisy temperature data in accordance to (12) to obtain $T_{f,i}, i = 0,1,\ldots,M$.
- Approximate heating/cooling rate $\frac{\partial T_f}{\partial t}(\eta,t)$ using filtered data via simple finite differences, though one could analytically obtain this through the filter.
- Numerically integrate (7b) to obtain the embedded heat flux, $q''(\eta,t)$.
- Approximate $\frac{\partial q''}{\partial t}(\eta,t)$ by a simple finite difference.
- Reconstruct Taylor series for both the surface temperature and heat flux using (14) and (15), respectively.

This process is proposed as a demonstation to indicate the merit of the concept. As noted by Frankel et al. [14], the higher time derivatives can contain substantially more error than the lower time derivatives and still render good results (as a consequence of a Taylor series). Key to this process is the digital filter and the choice of the cut-off frequency.

The heat flux, $q''(\eta,t)$, is approximated using Eq. 7b. As with most ill-posed functional equations, low-order numerical methods [9, pp. 67–76] are recommended for implementation. Let the discrete, noisy (corrupted) temperature data be denoted by $\{T_j\}_{j=0}^{M}$ corresponding to uniform sample times given by $\{t_j\}_{j=0}^{M}$ such that $t_j = j\Delta t$ where $\Delta t = t_{\max}/M$. To this end, a simple numerical procedure is offered that incorporates (7b) and the proposed Gauss filter. First, we discretize (7b), assuming that the heating/cooling rate, $\frac{\partial T}{\partial t}(0,t_j), j = 0,1,\ldots,M$, is known using a simple left-hand, rectangular product integration rule to obtain

$$q''_{f,i} = 2\sqrt{\frac{\rho Ck}{\pi}}\sum_{j=0}^{i-1}\frac{\mathrm{d}T_{f,j}}{\mathrm{d}t}(\sqrt{t_i - t_j} - \sqrt{t_i - t_{j+1}}), \quad i = 1,2,\ldots,M, \tag{18}$$

where we have expressed $\frac{\partial \bar{T}_f}{\partial t}(0,t_j) = \frac{\mathrm{d}T_{f,j}}{\mathrm{d}t}$ for notational simplicity. If $\frac{\mathrm{d}T_j}{\mathrm{d}t}$ is approximated using raw data, then the numerical results are unstable and inaccurate as M increases (or Δt decreases). Next, using a central-difference approximation, we form

$$\frac{\mathrm{d}T_{f,k}}{\mathrm{d}t} \approx \frac{T_{f,k+1} - T_{f,k-1}}{2\Delta t}, \quad k = 1,2,\ldots,M-1, \tag{19}$$

for the interior points and where we remind the reader that the subscript f denotes filtered. The final heating-rate condition is estimated with a backward difference (it is recognized that this is inconsistent with the interior discretization; however, it is in a region of little interest). Further, an initial steady-state condition is assumed which allows us to express the initial heating rate as $\mathrm{d}T_{f,\mathrm{o}}/\mathrm{d}t = 0$.

6 Numerical results

This section presents numerical results for the proposed inverse heat-conduction problem and numerical implementation. To demonstrate several key issues, consider the often-encountered heat flux of the Gaussian form [15]

$$q''(0,t) = q''_{\mathrm{o}}\mathrm{e}^{-(\frac{t-b}{\sigma})^2}, \quad t \geq 0, \tag{20}$$

where q''_o is the maximum heat-flux value acquired at $t = b$. The physical meanings for the parameters b and σ are self-evident. With this forcing function, we obtain "numerically exact" temperature data at the embedded location denoted as $x = \eta > 0$ through (3a). "Numerically exact" results for the embedded heat

flux, $q''(\eta,t)$, heating/cooling rate, $\frac{\partial T}{\partial t}(\eta,t)$, heat flux rate, $\frac{\partial q''}{\partial t}(\eta,t)$, etc can be estimated. For the present study, inexact, discrete data for the surface temperature $\{T_i\}_{i=1}^{M}$ are developed using Eq. 6 where we impose exactness on the initial condition, namely $T_o = T(\eta, t=0) = 0°C$.

For all calculations presented in this paper unless stated otherwise, it is assumed that $\eta = 0.3175\,\text{cm}$, $b = 0.75\,\text{s}$, $\sigma = 0.2\,\text{s}$, $q''_o = 25\,\text{MW/m}^2$, $k = 394\,\text{W/(mK)}$, and $\alpha = 114 \times 10^{-6}\,\text{m}^2/\text{s}$. The thermophysical properties are representative of copper. The embedded location, $x = \eta$, is at a physically reasonable distance from the surface. In fact, this value of η could be made smaller for real-world implementation without too much difficulty. For these plots, the discrete time, t_i, is defined using $t_i = i\Delta t$, $i = 1,2,\ldots,M$, where $\Delta t = t_{\max}/M$ and $t_{\max} = 2\,\text{s}$. Throughout this presentation, solid lines represent numerically "exact" results. Figure 3 ($M = 400, \gamma = 0$) displays numerically "exact" temperature and heat-flux distributions at $x = 0$ and $x = \eta$. From the temperature profile at $x = \eta$ discrete noisy data are developed through (6) and processed.

Figure 4 presents the required modified power spectra (Eq. (8f) when $N - 1 = M$) C_n over n for determining the critical or cut-off index, n_c or frequency, $f_c = n_c/t_{\max}$. From this figure, we estimate the cut-off index to be less than 45 or approximately 22.5 Hz. This figure shows the behavior of the power spectrum in the presence of ideal data and how n_c is visually estimated. The chosen numerical value is then used in Eq. (12) for obtaining the filtered temperature data denoted as $T_{f,i} = \bar{T}_{\text{filtered}}(t_i)$.

Next, let us investigate the situation where noise $\gamma = 0.015$ is added to the exact data displayed in Fig. 3 for the temperature, $T(\eta,t)$, in accordance to (6). Note, since $\|T(\eta,t)\|_\infty \approx 250°C$, the maximum local error is about $\pm 3.75°C$. Figure 5 displays the modified power spectra, C_n for these data when $M = 400$. This figure indicates a region where the cut-off value should be estimated. Let $n_c = 30$ for further calculations.

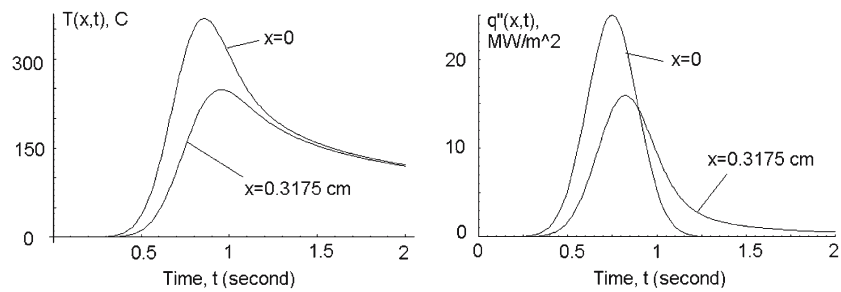

Fig. 3 Errorless temperature, $T(x,t)$ and heat flux $q''(x,t)$ at $x = 0$ and $x = \eta$ resulting from the imposed surface heat flux given in (18)

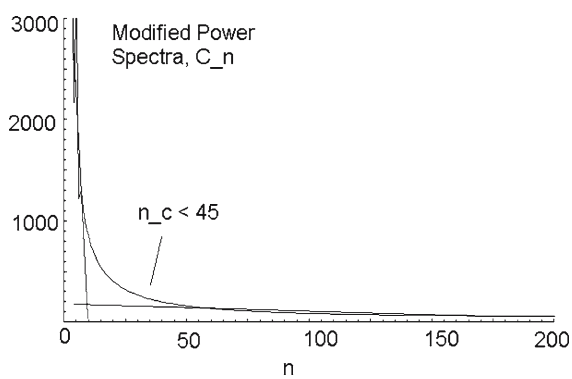

Fig. 4 Modified power spectra, C_n over increasing n required for estimating n_c based on Weiner (optimal) filtering concept in the presence of exact data

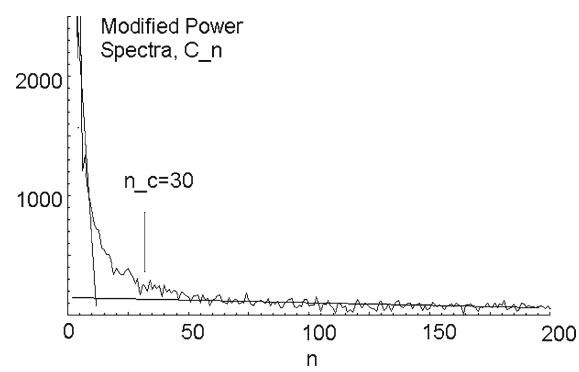

Fig. 5 Modified power spectra, C_n over increasing n for estimating n_c based on Weiner (optimal) filtering concept when noisy data are present

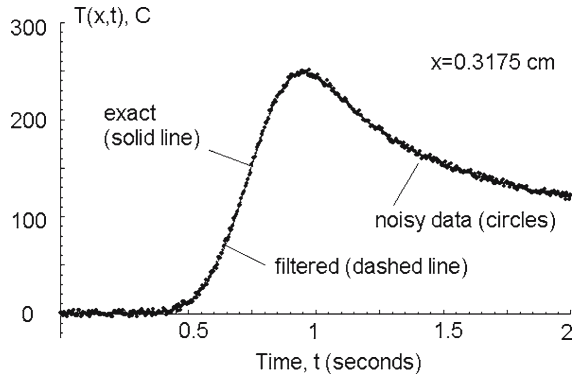

Fig. 6 Temperature $T(\eta, t)$ data: exact (solid line), noisy (solid circles) and filtered (dashed line)

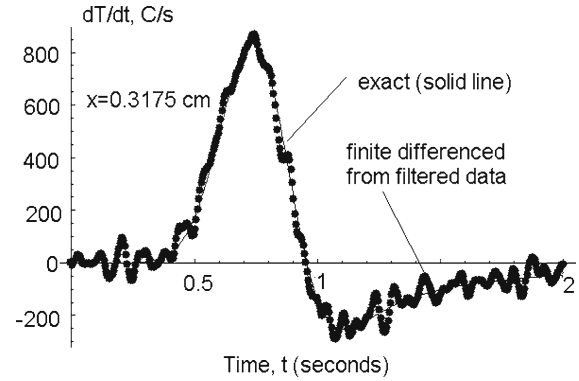

Fig. 7 Heating/cooling rate $\frac{\partial T}{\partial t}(\eta, t)$ data: exact (solid line), and predicted using filtered temperature data and central-difference representation for interior points

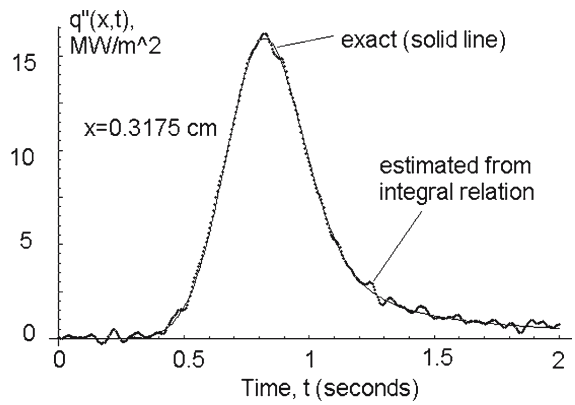

Fig. 8 Heat flux $q''(\eta, t)$ data: exact (solid line), and predicted using filtered temperature data (dashed line)

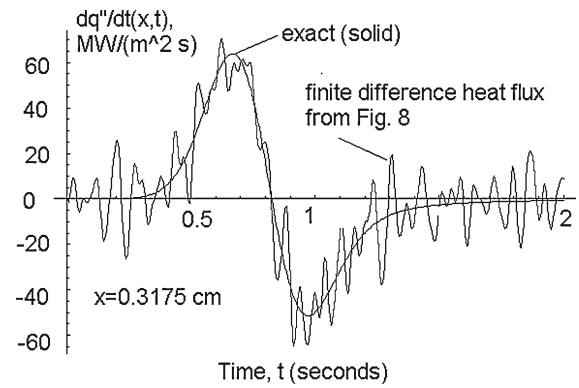

Fig. 9 Heat flux rate $\frac{\partial q''}{\partial t}(\eta, t)$ data: exact (solid line), and predicted using finite-difference approximation based on Fig. 8

Figure 6 presents the noisy data (solid circles) overlayed on the exact (solid line) and filtered data (dashed line) when $\gamma = 0.015$, $M = 400$. The filtered data are graphically indistinguishable from the exact curve. Figure 7 presents the heating/cooling rate, $\frac{\partial T}{\partial t}(\eta, t)$ based on the proposed finite differencing. Though the filtered temperature appears graphically exact, its time-derivative representation is deficient in accuracy. As the sample density, M, increases, one should expect a degradation in the rate representation, and hence the ill-posed nature of differentiation is identified. However, with this noted, these rate terms appear as higher-order terms of the Taylor series (see (14) and (15)) where each term is a correction to the low-order terms. Hence, these terms should be able to absorb additional errors.

Figure 8 presents the resulting heat-flux prediction, $q''(\eta, t)$, using the filtered data from Fig. 6 and the proposed numerical method based on (18). The heat flux is well predicted when compared to the "numerically" exact solution. Figure 9 presents the heat flux rate, $\frac{\partial q''}{\partial t}(\eta, t)$, based on the proposed simple finite-difference method. Again, the ill-posed nature of numerically differentiating noisy data is evident. Figures 10 and 11 present the projected surface temperature, $T(0, t)$, and heat flux, $q''(0, t)$, as additional terms are retained in their respective series representations per (14) and (15). Here, T1 = 1 term (leading), T2 = 2 terms, T3 = 3 terms, TN = N terms of the Taylor series displayed in (14). Here, Q1 = 1 term (leading), Q2 = 2 terms, Q3 = 3 terms, QN = N terms of the Taylor series displayed in (15). From these figures,

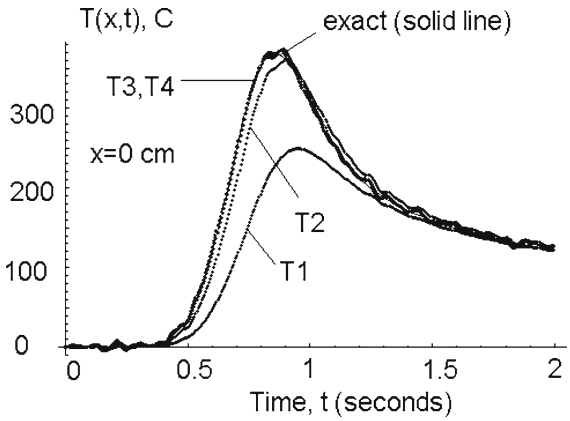

Fig. 10 Surface temperature predictions using (14) as the number of terms retained is increased

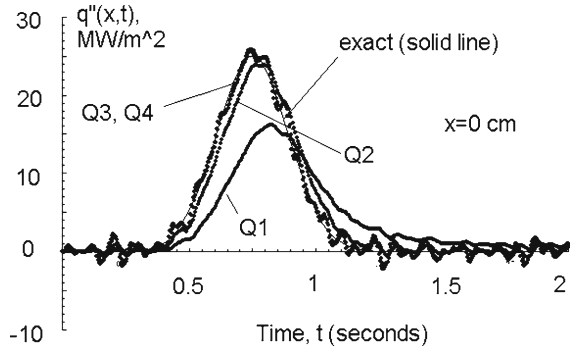

Fig. 11 Surface heat flux predictions using (15) as the number of terms retained is increased

Table 1 Root-mean-square error of the projected surface temperature and heat flux (at $x = 0$) over various cut-off indices, n_c (or equivalently cut-off frequencies, $f_c = n_c/t_{max}$) when $M = 400$

	$n_c = 20$	$n_c = 25$	$n_c = 30$	$n_c = 35$	$n_c = 40$
RMS error $T(0,t)$, (°C)	1.907	2.398	3.013	3.67	4.354
RMS error $q''(0,t)$, (MW/m^2)	0.4212	0.6350	0.8859	1.160	1.455

convergence appears to be taking place by order η^3 for the copper half-space where the data are collected at 0.3175 cm (or $1/8''$) from the active surface.

Table 1 provides some insight into the choice of cut-off frequency, f_c when $M = 400$, using copper in the half-space geometry previously defined for developing Figs. 10 and 11. The sample density of $M = 400$ is reasonable and its effect on the choice of n_c was described by Frankel and Arimilli [24]. For this study, focus is placed on the choice of the cut-off frequency based on fixed sampling rate, M. Up to this juncture, it is apparent that the direct measurement of higher-derivative terms could sustain higher errors than that of temperature or heat flux and still be effective in real-world situations. Again, the probe location is 0.3175 cm (or about $1/8''$) from the surface.

Table 1 presents the root-mean-square (RMS) error for both the surface temperature, $T(0,t)$, and heat flux, $q''(0,t)$, constructed from the Taylor series using T4 and Q4, respectively. Here, the RMS error, $\Delta\phi$ is defined as

$$\Delta\phi = \sqrt{\frac{\sum_{i=0}^{M}(\phi(t_i) - \phi_i)^2}{M+1}}, \tag{21}$$

where $\phi(t) =$ exact, and $\phi_i =$ measured value or reconstructed from the Taylor series. For this situation, $\phi(t)$ can take on the temperature, $T(0,t)$, or heat flux, $q''(0,t)$. The RMS error from both surface functions grows as the cut-off frequency increases for fixed sample density. This makes sense, since the filter is allowing additional high-frequency contamination to be retained (i.e., pass). However, graphical results for the resulting surface functions are not significantly altered. That is, although additional oscillations are added in the predictions as n_c is increased, the resulting histories do not change substantially in magnitude and thus significant flexibility exists in assigning this value. This is of considerable importance, since many classical regularization methods do not possess this latitude of adjustment. Again, the filter is based on the concept of signal-to-noise ratio which is a physically based criterion.

Table 2 Nomenclature

$a(x) = x^2/(4\alpha)$, s	T = Temperature, °C
C = Heat capacity, kJ/(kg°C)	T_o = Initial temperature, °C
k = Thermal conductivity, W/(m°C)	T_i = Discrete temperature, °C
q'' = Dimensional heat flux, W/m^2	u = Dummy variable, s
q''_{max} = Maximum heat flux, W/m^2	u_i = ith random number drawn
q''_i = Discrete heat flux, W/m^2	x = Spatial variable, m
$\dot{q}''_i$ = Discrete heat flux rate, W/(m^2 s)	*Greek*
M = Number of data points	α = Thermal diffusivity, m^2/s
N = Number of data	γ = Imposed noise level
s = Dummy variable, s	η = Fixed position, m
t = Time, s	λ = Constant $(1/\sqrt{k\rho C\pi})$
t_j = Discrete time, s	ω = Angular frequency
t_{max} = Maximum time, s	ρ = Density, kg/m^3
t_o = Dummy variable, s	

7 Conclusions

This paper conveys the need for and benefit of the direct measurement or interpretation for higher-time derivatives of temperature and heat flux for inverse analysis. These fundamental findings should stimulate interest and serve to motivate the development of rate-based thermal sensors for real-time inverse heat-conduction analysis as displayed by the Taylor series. The appendices provide derivations germane to the equations used in the body of the paper and clarify the integral relation between temperature and heat flux in the half-space, as well as providing some insight into the hypersingular nature of the problem. Finally, the numerical methods used in this paper are intentionally chosen to be simple while the important feature is the proper filtering of the data or developing rate sensors. Additionally, Frankel et al. [32] have developed a rate interface that is applicable to both temperature and heat flux for providing time derivative information. Frankel et al. [32] have performed a series of thermocouple experiments for demonstrating this new technology (Table 2).

Appendix A. Integral relationship between temperature and heat flux from Equation 3a

The relationship that Kulish and his coworkers developed is actually available in the solution of the heat equation displayed in (3a) (where the initial condition is now assumed nontrivial) and its complementary flux solution displayed in (3b), i.e.,

$$T(x,t) = T_o + \sqrt{\frac{1}{\rho Ck\pi}} \int_{u=0}^{t} q''(0,u) \frac{e^{-\frac{x^2}{4\alpha(t-u)}}}{\sqrt{t-u}} du, \quad (x,t) \geq 0, \tag{22}$$

$$q''(x,t) = \sqrt{\frac{x^2}{4\alpha\pi}} \int_{u=0}^{t} q''(0,u) \frac{e^{-\frac{x^2}{4\alpha(t-u)}}}{(t-u)^{\frac{3}{2}}} du, \quad x > 0, \ t \geq 0, \tag{23}$$

respectively. This is important to demonstrate, since the Fourier-cosine transform method can be viewed as a Green's function formulation in some sense.

To develop the relationship shown in (7b), which is equivalent to the inverted form of (7a), we follow a regularization procedure associated with weakly singular integral equations. Let $t \to s$ in (22), operate on the result with $\frac{ds}{\sqrt{t-s}}$ and integrate to obtain

$$\int_{s=0}^{t} \frac{T(x,s)}{\sqrt{t-s}} ds = T_o \int_{s=0}^{t} \frac{ds}{\sqrt{t-s}} + \frac{1}{\sqrt{\rho Ck\pi}} \int_{s=0}^{t} \int_{u=0}^{s} q''(0,u) \frac{e^{-\frac{x^2}{4\alpha(s-u)}}}{\sqrt{t-s}\sqrt{s-u}} du\, ds. \tag{24}$$

Next, interchange orders of integration on the triangle, and noting

$$\int_{s=u}^{t} \frac{\mathrm{e}^{-\frac{x^2}{4\alpha(s-u)}}}{\sqrt{t-s}\sqrt{s-u}}\mathrm{d}s = \pi\left(1-\mathrm{erf}\sqrt{\frac{a(x)}{t-u}}\right), \tag{25}$$

where $a(x) = x^2/(4\alpha)$ and erf (z) is the error function having argument z, we arrive at

$$\int_{u=0}^{t} \frac{T(x,u)}{\sqrt{t-u}}\mathrm{d}u = 2T_{\mathrm{o}}\sqrt{t} + \sqrt{\frac{\pi}{\rho Ck}}\int_{u=0}^{t} q''(0,u)\left(1-\mathrm{erf}\sqrt{\frac{a(x)}{t-u}}\right)\mathrm{d}u, \tag{26}$$

where we let $s \to u$ in the LHS for notational simplicity. Integrating the LHS by parts and differentiating the resulting equation with the aid of Leibnitz's rule produces

$$\int_{u=0}^{t} \frac{\partial T}{\partial u}(x,u)\frac{\mathrm{d}u}{\sqrt{t-u}} = \frac{x}{2k}\int_{u=0}^{t} q''(0,u)\frac{\mathrm{e}^{-\frac{a(x)}{t-u}}}{(t-u)^{\frac{3}{2}}}\mathrm{d}u, \tag{27}$$

where

$$\frac{\partial}{\partial t}\,\mathrm{erf}\sqrt{\frac{a(x)}{t-u}} = -\sqrt{\frac{a(x)}{\pi}}\frac{\mathrm{e}^{\frac{-a(x)}{t-u}}}{(t-u)^{\frac{3}{2}}},$$

and since erf $(\infty) = 1$. However, we recognize a portion of the RHS in (27) from (23). Eliminating the integral in the RHS of (27) using (23) produces the desired relationship shown in (7b), namely

$$q''(x,t) = \sqrt{\frac{\rho Ck}{\pi}}\int_{u=0}^{t} \frac{\partial T}{\partial u}(x,u)\frac{\mathrm{d}u}{\sqrt{t-u}}, \quad t \geq 0. \tag{28}$$

This process can be generalized and used in conjunction with Green's functions. To return to (7a), we merely perform a similar regularization process as outlined previously.

Appendix B. Integral relationships by the Green's function method

The Boundary Element Method (BEM) involves the classical Green's function approach but is based on a full-space Green's function for all geometries [33, pp. 141–150]. The method begins by operating on the heat equation given as

$$\frac{1}{\alpha}\frac{\partial T}{\partial t}(x,t) = \frac{\partial^2 T}{\partial x^2}(x,t), \quad (x,t) \geq 0, \tag{29}$$

with the Green's function is denoted as $G(x,t/x_{\mathrm{o}},t_{\mathrm{o}})$. Here, G(effect/cause) notation is used [19,34]. Doing so and integrating over the spatial and temporal domains of interest, we obtain

$$\lim_{\epsilon\to 0}\int_{t_{\mathrm{o}}=0}^{t+\epsilon}\int_{x_{\mathrm{o}}=0}^{\infty}\left(\frac{1}{\alpha}\frac{\partial T}{\partial t_{\mathrm{o}}}(x_{\mathrm{o}},t_{\mathrm{o}}) - \frac{\partial^2 T}{\partial x_{\mathrm{o}}^2}(x_{\mathrm{o}},t_{\mathrm{o}})\right)G(x,t/x_{\mathrm{o}},t_{\mathrm{o}})\mathrm{d}x_{\mathrm{o}}\mathrm{d}t_{\mathrm{o}} = 0, \quad (x,t) \geq 0, \tag{30}$$

where causality is noted through the limit displayed in (30). Integrating by parts, making use of causality, the conditions at infinity, and the known initial (trivial) condition reduces (30) to

$$w_x T(x,t) = -\int_{t_{\mathrm{o}}=0}^{t}[G(x,t/0,t_{\mathrm{o}})\frac{\partial T}{\partial x_{\mathrm{o}}}(0,t_{\mathrm{o}}) - G_{x_{\mathrm{o}}}(x,t/0,t_{\mathrm{o}})T(0,t_{\mathrm{o}})]\mathrm{d}t_{\mathrm{o}}, \quad (x,t) \geq 0, \tag{31a}$$

where w_x is a weight function and the Green's function [33] is determined from the solution of

$$\frac{1}{\alpha}\frac{\partial G}{\partial t_{\mathrm{o}}} + \frac{\partial^2 G}{\partial x_{\mathrm{o}}^2} = -\delta(x_{\mathrm{o}}-x)\delta(t_{\mathrm{o}}-t), \quad (x,x_{\mathrm{o}}) \in (-\infty,\infty), \;\; t_{\mathrm{o}} > t, \tag{31b}$$

subject to regularity conditions at ±infinity and causality. This Green's function is constructed by use of the adjoint operator and thus is backwards in time. Equation 31b defines the full-space Green's function and thus requires the introduction of w_x in (31a). At $x = 0$, $w_0 = 0.5$, otherwise it is set to unity. The full-space Green's function is given by [34, p. 100]

$$G(x,t/x_o,t_o) = \sqrt{\frac{\alpha}{4\pi(t-t_o)}}\,e^{-\frac{(x-x_o)^2}{4\alpha(t-t_o)}}, \quad (x,x_o) \in (-\infty,\infty), \;\; t > t_o. \tag{31c}$$

The development of the Green's function in the causal variable is indicated here, though most books develop the Green's function in the effect variable (and thus the adjoint operator displayed in (31b) is replaced by the heat operator shown in (29) based on reciprocity).

Evaluating Eq. at $x = 0$ produces

$$T(0,t) = \frac{1}{\sqrt{\rho Ck\pi}}\int_{t_o=0}^{t}\frac{q''(0,t_o)}{\sqrt{t-t_o}}\mathrm{d}t_o, \quad t \geq 0, \tag{32}$$

since $q''(0,t) = -k\frac{\partial T}{\partial x}(0,t)$ and $w_0 = 1/2$. Inversion of (32), as previously described, produces

$$q''(0,t) = \sqrt{\frac{\rho Ck}{\pi}}\int_{t_o=0}^{t}\frac{\partial T}{\partial t_o}(0,t_o)\frac{\mathrm{d}t_o}{\sqrt{t-t_o}}, \quad t \geq 0. \tag{33}$$

Next, we can develop a generalized methodology for arriving at (7b) based on the Green's function approach. This is significant, since it can be generalized to finite-width slabs for the first time [28]. The derivation parallels the concept first introduced in Appendix A. To begin, let us explicitly express the temperature distribution displayed in (31a) as

$$w_x T(x,t) = \frac{1}{\sqrt{4\pi\rho Ck}}\int_{t_o=0}^{t} q''(0,t_o)\frac{e^{-\frac{x^2}{4\alpha(t-t_o)}}}{\sqrt{t-t_o}}\mathrm{d}t_o + \frac{x}{4\sqrt{\alpha\pi}}\int_{t_o=0}^{t} T(0,t_o)\frac{e^{-\frac{x^2}{4\alpha(t-t_o)}}}{(t-t_o)^{\frac{3}{2}}}\mathrm{d}t_o. \tag{34}$$

If we operate on (34) with $-k\frac{\partial}{\partial x}$ and recall the definition of the heat flux through Fourier's law as $q''(x,t) = -k\frac{\partial T}{\partial x}(x,t)$, we arrive at

$$w_x q''(x,t) = \sqrt{\frac{\rho Ck}{\pi}}\left\{\frac{x}{4k}\int_{t_o=0}^{t} q''(0,t_o)\frac{e^{-\frac{x^2}{4\alpha(t-t_o)}}}{(t-t_o)^{\frac{3}{2}}}\mathrm{d}t_o + \frac{1}{4}\int_{t_o=0}^{t} T(0,t_o)\left[\frac{x^2}{2\alpha}\frac{e^{-\frac{x^2}{4\alpha(t-t_o)}}}{(t-t_o)^{\frac{5}{2}}} - \frac{e^{-\frac{x^2}{4\alpha(t-t_o)}}}{(t-t_o)^{\frac{3}{2}}}\right]\mathrm{d}t_o\right\}. \tag{35}$$

Observe at $x = 0$, Equation (35) reduces to the hypersingular equation [35–38]

$$q''(0,t) = -\sqrt{\frac{\rho Ck}{4\pi}}\int_{t_o=0}^{t}\frac{T(0,t_o)}{(t-t_o)^{\frac{3}{2}}}\mathrm{d}t_o, \tag{36}$$

which is discussed further in Appendix C. Though the apparent inversion now appears to only involve the surface temperature and the hypersingular kernel, this allusion must be well understood (i.e., the operator which it comes from). That is, the resulting equation is still ill-posed when contaminated surface temperature data are present.

For notational convenience, let $t_o \to u$ and then we begin the regularization process by letting $t \to s$ and operate on the resulting expression with $\mathrm{d}s/\sqrt{t-s}$ followed by integration over the domain of interest to get

$$\begin{aligned} w_x\int_{s=0}^{t}\frac{T(x,s)}{\sqrt{t-s}}\mathrm{d}s = {} & \frac{1}{\sqrt{4\pi\rho Ck}}\int_{s=0}^{t}\int_{u=0}^{s} q''(0,u)\frac{e^{-\frac{x^2}{4\alpha(s-u)}}}{\sqrt{t-s}\sqrt{s-u}}\mathrm{d}u\;\mathrm{d}s \\ & + \frac{x}{4\sqrt{\alpha\pi}}\int_{s=0}^{t}\int_{u=0}^{s} T(0,u)\frac{e^{-\frac{x^2}{4\alpha(s-u)}}}{\sqrt{t-s}(s-u)^{\frac{3}{2}}}\mathrm{d}u\;\mathrm{d}s, \quad (x,t) \geq 0. \end{aligned} \tag{37}$$

Carefully interchanging orders of integration on the triangle permits the reduction of (37) to

$$w_x \int_{s=0}^{t} \frac{T(x,s)}{\sqrt{t-s}}\mathrm{d}s = \frac{\sqrt{\pi}}{\sqrt{4\rho Ck}}\left(\int_{u=0}^{t} q''(0,u)\mathrm{d}u - \int_{u=0}^{t} q''(0,u)\,\mathrm{erf}\left(\sqrt{\frac{x^2}{4\alpha(t-u)}}\right)\mathrm{d}u\right)$$
$$+\frac{1}{2}\int_{u=0}^{t} T(0,u)\frac{\mathrm{e}^{-\frac{x^2}{4\alpha(t-u)}}}{\sqrt{t-u}}\mathrm{d}u, \quad (x,t) \geq 0, \tag{38a}$$

where

$$\int_{s=u}^{t} \frac{\mathrm{e}^{-\frac{x^2}{4\alpha(s-u)}}}{\sqrt{t-s}\sqrt{s-u}}\mathrm{d}s = \pi\left(1-\mathrm{erf}\left(\sqrt{\frac{x^2}{4\alpha(t-u)}}\right)\right), \tag{38b}$$

$$\int_{s=u}^{t} \frac{\mathrm{e}^{-\frac{x^2}{4\alpha(s-u)}}}{\sqrt{t-s}(s-u)^{\frac{3}{2}}}\mathrm{d}s = \sqrt{\frac{4\pi\alpha}{x^2}}\frac{\mathrm{e}^{-\frac{x^2}{4\alpha(t-u)}}}{\sqrt{t-u}}. \tag{38c}$$

Next, we let $s \to u$ for notational balance (i.e., cosmetics) integrate the LHS of (38a) by parts and incorporate the trivial initial condition to obtain

$$2w_x \int_{u=0}^{t} \sqrt{t-u}\frac{\partial T}{\partial u}(x,u)\mathrm{d}u = \frac{\sqrt{\pi}}{\sqrt{4\rho Ck}}\left(\int_{u=0}^{t} q''(0,u)\mathrm{d}u - \int_{u=0}^{t} q''(0,u)\,\mathrm{erf}\left(\sqrt{\frac{x^2}{4\alpha(t-u)}}\right)\mathrm{d}u\right)$$
$$+\frac{1}{2}\int_{u=0}^{t} T(0,u)\frac{\mathrm{e}^{-\frac{x^2}{4\alpha(t-u)}}}{\sqrt{t-u}}\mathrm{d}u, \quad (x,t) \geq 0, \tag{39a}$$

and then differentiate this result with respect to time using Leibnitz's rule to obtain

$$w_x \int_{u=0}^{t} \frac{\partial T}{\partial u}(x,u)\frac{\mathrm{d}u}{\sqrt{t-u}} = \frac{x}{4k}\int_{u=0}^{t} q''(0,u)\frac{\mathrm{e}^{-\frac{x^2}{4\alpha(t-u)}}}{(t-u)^{\frac{3}{2}}}\mathrm{d}u + \frac{1}{4}\int_{u=0}^{t} T(0,u)\left(\frac{x^2}{2\alpha}\frac{\mathrm{e}^{-\frac{x^2}{4\alpha(t-u)}}}{(t-u)^{\frac{5}{2}}} - \frac{\mathrm{e}^{-\frac{x^2}{4\alpha(t-u)}}}{(t-u)^{\frac{3}{2}}}\right)\mathrm{d}u, \tag{39b}$$

for $(x,t) \geq 0$. Comparing (35) with (39b), we can make the final identification of the heat flux in the RHS of (39b) and hence arrive at

$$q''(x,t) = \sqrt{\frac{\rho Ck}{\pi}}\int_{u=0}^{t} \frac{\partial T}{\partial u}(x,u)\frac{\mathrm{d}u}{\sqrt{t-u}}, \quad (x,t) \geq 0. \tag{40}$$

Frankel [28] has demonstrated, for the first time, that the heat equation governed in (1a) for a finite slab produces the identical integral relationship between the local temperature and heat flux based on the Green's function approach.

Appendix C. Hypersingular equation, Equation 36

Some initial background and definitions are presented in the context of hypersingular integrals [35, pp. 464–468, 36–38]. To begin, by way of example, using a classical strongly singular kernel, we introduce the definition of hypersingularity. Let the function $\Phi(x) \in C^1[a,b]$. Consider the improper integral on the interval $[a,b]$ such that (i) the integrand has a singularity of the type $\frac{1}{(x-y)^2}$ at the interior point y, $a < y < b$ and (ii) the regular part of the integrand is a function that satisfies a Hölders continuous first-derivative condition

$$|\Phi(x) - \Phi(y) - (x-y)\Phi'(y)| \leq A|x-y|^{\beta+1}, \tag{41}$$

such that $\Phi'(y) = \frac{d\Phi}{dy}$, $0 < \beta \leq 1$ and $|A| < \infty$, then a Hadamard (finite part) integral is defined by

$$\oint_a^b \frac{\Phi(x)}{(x-y)^2}\mathrm{d}x = \lim_{\epsilon\to 0}\left[\left(\int_a^{y-\epsilon} + \int_{y+\epsilon}^b\right)\frac{\Phi(x)}{(x-y)^2}\mathrm{d}x - \frac{2\Phi(y)}{\epsilon}\right]. \tag{42}$$

Note that differentiation of a Cauchy Principal Value integral (via Leibnitz's rule) produces

$$\frac{\mathrm{d}}{\mathrm{d}y}\int_a^b \frac{\Phi(x)}{x-y}\mathrm{d}x = \oint_a^b \frac{\Phi(x)}{(x-y)^2}\mathrm{d}x, \tag{43}$$

which is often used as the definition of a finite-part integral.

As a basic example more in line with the present study, consider

$$S_{\mathrm{o}}(x) = \int_a^x \frac{\mathrm{d}t}{(x-t)^{\frac{1}{2}}} = -2(x-t)^{\frac{1}{2}}|_a^x = 2(x-a)^{\frac{1}{2}}. \tag{44}$$

Differentiation of $S_{\mathrm{o}}(x)$ with respect to x on both sides separately yields

$$\frac{\mathrm{d}S_o}{\mathrm{d}x}(x) = -\frac{1}{2}\int_a^x \frac{\mathrm{d}t}{(x-t)^{\frac{3}{2}}} + \frac{1}{(x-t)^{\frac{1}{2}}}|_{t\to x} = \frac{1}{\sqrt{x-a}}. \tag{45}$$

It is seen that the derivative of $S_{\mathrm{o}}(x)$ (which is bounded) is the difference between a divergent integral and an unbounded integrated term. Noting that the integrated term is independent of "a", we may consider the derivative of $S_{\mathrm{o}}(x)$ as being the "finite part" of the divergent integral and define

$$\oint_a^x \frac{\mathrm{d}t}{(x-t)^{\frac{3}{2}}} = \lim_{c\to x}\left(\int_a^c \frac{\mathrm{d}t}{(x-t)^{\frac{3}{2}}} - \frac{2}{\sqrt{c-t}}\right) = -\frac{2}{\sqrt{x-a}}. \tag{46}$$

For numerically evaluating the integral displayed by (42), we take advantage of singularity subtraction [20] and consideration of Hölder's condition displayed in (41). That is, we express the LHS of Eq. 42 as

$$\begin{aligned}\oint_a^b \frac{\Phi(x)}{(x-y)^2}\mathrm{d}x = &\int_a^b [\Phi(x) - \Phi(y) - (x-y)\Phi'(y)]\frac{\mathrm{d}x}{(x-y)^2} + \Phi(y)\oint_a^b \frac{\mathrm{d}x}{(x-y)^2}\\ &+\Phi'(y)\oint_a^b \frac{\mathrm{d}x}{x-y}, \quad y \in (a,b),\end{aligned} \tag{47}$$

where $\Phi \in C^2(a,b)$. Note that the integrand is now bounded at $x = y$ (via l'Hôpital's rule) and approaches $0.5\Phi''(y)$ as $x \to y$.

Let us now return to (36) with a new interpretation. That is, let us use singularity subtraction and Hölder's condition (basically a two-term Taylor series about $t_{\mathrm{o}} = t$) to rewrite (36) as

$$\begin{aligned}q''(0,t) = -\frac{\sqrt{\rho Ck}}{\sqrt{4\pi}}\Bigg\{&\int_{t_{\mathrm{o}}=0}^t \left[T(0,t_{\mathrm{o}}) - T(0,t) + (t-t_{\mathrm{o}})\frac{\partial T}{\partial t}(0,t)\right]\frac{\mathrm{d}t_{\mathrm{o}}}{(t-t_{\mathrm{o}})^{\frac{3}{2}}}\\ &+T(0,t)\oint_{t_{\mathrm{o}}=0}^t \frac{\mathrm{d}t_{\mathrm{o}}}{(t-t_{\mathrm{o}})^{\frac{3}{2}}} - \frac{\partial T}{\partial t}(0,t)\int_{t_{\mathrm{o}}=0}^t \frac{\mathrm{d}t_{\mathrm{o}}}{\sqrt{t-t_{\mathrm{o}}}}\Bigg\},\end{aligned} \tag{48}$$

or

$$q''(0,t) = -\frac{\sqrt{\rho Ck}}{\sqrt{4\pi}}\left\{\int_{t_{\mathrm{o}}=0}^t \left[T(0,t_{\mathrm{o}}) - T(0,t) + (t-t_{\mathrm{o}})\frac{\partial T}{\partial t}(0,t)\right]\frac{\mathrm{d}t_{\mathrm{o}}}{(t-t_{\mathrm{o}})^{\frac{3}{2}}} - \frac{2T(0,t)}{\sqrt{t}} - 2\sqrt{t}\frac{\partial T}{\partial t}(0,t)\right\}. \tag{49}$$

Equation 49 seems well prepared for a simple numerical quadrature if presented both temperature and heating/cooling-rate data. It is interesting to note that this formulation makes use of the entire temperature data set but only requires the last heating/cooling-rate value. Again, this formulation clearly indicates that (36) is ill-posed since differentiated data are still required. Any simple numerical quadrature rule is sufficient to yield accurate results if control on the heating/cooling-rate term is maintained as the sample density increases. Thus, filtering, as described in this paper, works well on this alternative formulation, even when using a left-hand rectangular product integration rule and a simple central-difference to represent the time derivative. The equation described in (49) is similar to that developed by Cook and Felderman [39].

References

1. Doebelin EO (1975) Measurement systems. McGraw-Hill, New York
2. Diller TE (1993) Advances in heat flux measurements. Vol. 23, Academic Press, New York, pp 279–368
3. Keltner NR (1997) Heat flux measurements: theory and applications. In: Keltner NR (ed) Thermal measurements in electronic cooling. CRC, New York, pp 273–320
4. Holman JP (1984) Experimental methods for engineers, 4th ed., McGraw Hill, New York
5. Kress R (1989) Linear integral equations. Springer-Verlag, Berlin
6. Wing GM (1991) A primer on integral equations of the first kind. SIAM, Philadelphia
7. Beck JV, Blackwell B, St. Clair CR, Jr (1985) Inverse heat conduction. Wiley, New York
8. Kurpisz K, Nowak AJ (1995) Inverse thermal problems. Computational Mechanics, Southampton
9. Linz P (1985) Analytical and numerical methods for Volterra equations. SIAM, Philadelphia
10. Baker CTH (1978) The numerical treatment of integral equations. Clarendon Press, Oxford
11. Frankel JI, Keyhani M, Taira K (2004) In-phase error estimation of experimental data and optimal first derivatives. AIAA J 42: 1017–1024
12. Frankel JI, Keyhani M (1999) Inverse heat conduction: The need of $\frac{\partial T}{\partial t}$ data for design and diagnostic purposes. In: IASTED MIC 99, Innsbruck, Austria
13. Frankel JI (2000) Inverse heat conduction and data-type issues. Boun Elem Commun 11:37–42
14. Frankel JI, Osborne GE, Taira K (2006) Stabilization of ill-posed problems through thermal rate sensors. AIAA J Thermophys Heat Trans 20:238–246
15. Frankel JI, Lawless JJ (2005) Numerically stabilizing ill-posed moving surface problems through heat rate sensors. AIAA J Thermophys Heat Trans 19:587–592
16. Frankel JI, Osborne GE (2004) Motivation for the development of heating/cooling rate dT/dt and heat flux rate dq″/dt sensors for engineering applications. In: 42nd AIAA Aerospace sciences meeting and exhibit, Reno, NV, January 5–8.
17. Frankel JI (2005) Heating/cooling rate sensor development for stable, real-time heat flux predictions. 43rd AIAA Aerospace sciences meeting and exhibit, Reno, NV, January 10–13
18. Ozisik MN (1980) Heat conduction. Wiley, New York
19. Frankel JI, Vick B, Ozisik MN (1985) Flux formulation in hyperbolic heat conduction. J Appl Phys 58:3340–3345
20. Frankel JI (1991) Nonlinear heat transfer: solution of singular, nonlinear integral equations. Eng Anal 8:231–238
21. Hildebrand FB (1976) Advanced calculus for applications, 2nd ed., Prentice Hall, Englewood Cliffs
22. Hanke M, Scherzer O (2001) Inverse problems light: numerical differentiation. Amer Math Monthly 108:512–520
23. Groetsch T (1991) Differentiation of approximately specified functions. Amer Math Monthly 98:847–850
24. Frankel JI, Arimilli RV (in press) Inferring convective and radiative heating loads from transient surface temperature measurements in the half-space. Inverse Prob Sci Eng
25. Stakgold I (1979) Green's functions and boundary value problems. Wiley, New York
26. Kulish VV, Novozhilov VB (2003) Integral equation for the heat transfer with the moving boundary. AIAA J Thermophys Heat Trans 17:538–540
27. Kulish VV, Lage JL (2000) Fractional diffusion solutions for transient local temperature and heat flux. Heat Trans 122:372–376
28. Frankel JI (2006) Generalizing the method of Kulish to one-dimensional unsteady heat conducting slabs. J Thermophys Heat Trans 20:945–950
29. Briggs WL, Henson VE (1995) The DFT. SIAM, Philadelphia
30. Press WH, Flannery BP, Teukolsky SA, Vetterling WT (1986) Numerical recipes. Cambridge University Press, Cambridge
31. Hamming RW (1989) Digital filters, 3rd ed. Dover, New York
32. Frankel JI, Arimilli RV, Keyhani M, Wu J (2006) Heating rate dT/dt measurements developed from in-situ thermocouples using a voltage-rate interface for advanced thermal diagnostics. In: 25th AIAA Aerodynamics measurement technology ground testing conference, San Francisco, June 5–8
33. Brebbia CA, Telles JCF, Wrobel LC (1984) Boundary element techniques. Springer-Verlag, New York
34. Greenberg MD (1971) Applications of Green's functions in science and engineering. Prentice-Hall, Englewood Cliffs
35. Kythe PK, Puri P (2002) Computational methods for linear integral equations. Birkhauser, Boston
36. Martin PA (1992) Exact solution of a simple hypersingular integral equation. J Int Equ Applic 4:197–204
37. Kaya AC, Erdogan F (1987) On the solution of integral equations with strongly singular kernels. Q Appl Math 45:105–122
38. Monegato G (1994) Numerical evaluation of hypersingular integrals. J Comp Appl Math 50:9–31
39. Cook WJ, Felderman EJ (1966) Reduction of data from thin-film heat transfer gages: a concise numerical technique. AIAA J 4:561–562